IJMSIT

International Journal of Multidisciplinary Studies and Innovative Technologies

Volume : 2
Number: 2
Year: 2018
Pages: 43 - 50

MULTIPHYSICS NUMERICAL ANALYSIS OF MR DAMPER WITH EXPERIMENTAL VALIDATION

Zekeriya PARLAK*[1], Mustafa Ertürk SÖYLEMEZ[2], Muaz Kemerli[1] and İsmail Şahin[3]

[1]*Sakarya University Engineering Faculty Mechanical Engineering Department, Sakarya, Turkey*
[2]*Muş Alparslan University, Engineering and Architectural Faculty, Mechanical Engineering Department, Muş, Turkey*
[3]*Sakarya Applied Sciences University, Akyazı Vocational School, Sakarya, Turkey*
**zparlak@sakarya.edu.tr*

Abstract **–** Multiphysics numerical analysis , which are the magnetic field and time-dependent CFD analysis, validated by experimental results have been performed to obtain the magnetic flux density and relationship of damping force-displacement. The most effective levels of the design parameters have been determined regarding of the damping force and dynamic range. Also, the expected performances of the optimal MR damper designs and effect each design parameter on performance have been calculated statistically corresponding to different velocity values. Results showed that, from 0.05 m/s to 0.15 m/s of piston velocity, the effect of the gap width was increased by 2.56% while the active length was decreased by 4.12% under constant current.

Keywords – Magnetorheological damper; Design of experimental; Time-dependent CFD analysis; non-Newtonian flow; Coupled analysis; Moving boundaries

I. INTRODUCTION

An MR damper basically consists of a cylinder, a piston head wrapped around a coil, a piston shaft, and sealing elements. Manufacturing an MR damper that best suits the operating conditions, requires numerical modeling and testing.

Optimization studies of MR damper design parameters have received many interests and many authors have studied numerically and experimentally. Hitchcock (2002) carried out the 3D FEM analysis with ANSOFT software to find optimum values for magnetic field direction and intensity. Rosenfeld and Wereley (2004) compared the performance of the optimized MR valve with similar ER valve using both analytical and numerical techniques. Nguyen et al. (2007) provided a convergence on design variables such as magnetic flux density, pressure drop and dynamic range, taking into account the constant values of diameter and length of the MR valve cylinder, fluid viscosity, flow rate and channel width, so that they obtained optimal values such as valve housing thickness, coil width. Karakoc et al. (2008) obtained optimum values of the design parameters of an automotive MR brake with the optimization algorithm. At the same time, an FEM analysis was presented to analyze magnetic field and heating within the MR brake. Erol and Gurocak (2011) obtained the optimal configuration of the MR brake including parameters such as current, coil winding number and coil wire diameter. Azraai et al. (2015) used Particle Swarm Optimization (PSO) method to optimize parameters of the MR dampers. Hu et al. (2016) an FEM was built to work the performance of the double coil MR damper by investigating seven different piston configurations, and they obtained the optimal damping performance of the damper by using the APDL. In our previous study (Parlak et al., 2013) the optimal MR damper configurations were obtained by using Taguchi experimental design method without taking into account temperature rise and applied current is one of four design parameters. Scientists (Rosenfeld and Wereley, 2004; Nguyen et al., 2007; Karakoc et al., 2008; Ozan and Gurocak, 2011; Azraai et al., 2015; Hu et al., 2016; Parlak et al., 2013) have emphasized on the importance of optimizing the MR device and their numerical and experimental findings have been presented comparatively. Although these results provide a significant contribution to the literature, they have not developed models which consider temperature rise in the damper operation and they have not considered different current excitation conditions in the optimization works.

Some studies have been presented by several researchers for MR fluid and MR damper modeling using numerical analysis (Kemerli et al., 2019, Parlak and Engin, 2012, Sternberg et al., 2014, Zheng et al., 2015). In the numerical models, Navier–Stokes and/or Maxwell equations are solved numerically for MR fluid flow and magnetic field.

By making appropriate design that meet the expected working conditions or to provide controlling model of the MR damper, an appropriate numerical model closest to the test data can be developed. A few studies have been examined the effects of heating during operation on the damper. Yu et al. (2015) established a theoretical model of temperature change on a kind of self-decoupling magnetorheological (SDMR)

damper based on conservation of energy. Zhu et al. (2015) proposed a MR damper which can provide both damping effect and recycling energy from mechanical vibration. Thirupathi et al. (2015) have conducted tests with a simple MR damper for a new MR fluid produced.

The current study aims; (1) to determine the most effective MR damper design by performing experiments under constant temperature by method of the design of experimental , (2) to reveal the adverse effect of temperature rise on the MR fluid, (3) to show most effective levels and impact of design parameters on performance corresponding to different velocity values (4) to obtain the magnetic flux density and relationship of damping force-displacement by multiphysics numerical analysis, which are the magnetic field and time-dependent CFD analysis and (5) to visualize of the magnetic field and fluid flow in MR damper by numerical analysis.

II. EXPERIMENTAL DESIGN OF MR DAMPER

An MR damper basically consists of a cylinder, a piston head wrapped around a coil, a piston shaft, and sealing elements. MR fluid can pass to the other side of the cylinder through the narrow channel (gap) on the piston head (Fig 1). When high pressured MR fluid is forced along a gap, frictional losses caused by the resistance to flow occur and cause pressure drop in the MR damper. The force along the narrow channel is activated by a magnetic field due to current carrying circular coil. Also, in the MR dampers, an accumulator, which is filled with the pressurized gas such as nitrogen, is used for compensating the volume changes induced by the movement of the piston rod in the cylinder. On the other hand, temperature rise is caused by the mechanical friction and the heating of the coil and it significantly reduces the viscosity of the MR fluid and thus, the damper cannot provide the expected damping force. In this case, either MR dampers must be cooled or the effect of temperature rise on fluid viscosity in the calculations must be considered by making appropriate design that meet the expected working conditions or to provide controlling model of the MR damper. In the current study, MR damper temperature is kept constant by experimentally (detailed in section 3) and damper design is done by following optimization procedure similar to in our previous studies (Parlak et al., 2013).

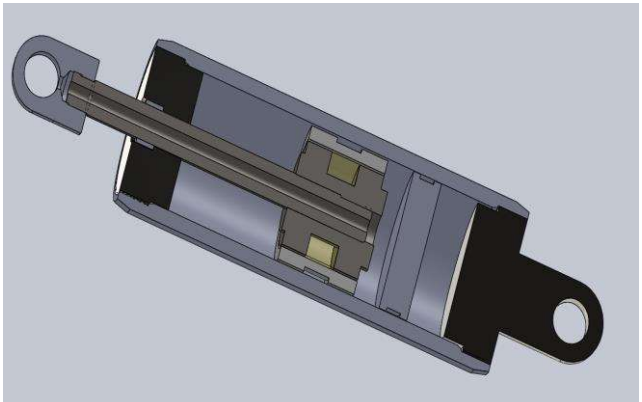

Fig. 1 Cross-Section of MR damper

The dimensions of the magnetic circuit of the MR damper, which characterize by the annular gap width, g, the gap length, L, thickness of the piston head housing, g_h, t_k, the piston head radius, R, the piston core radius, R_c and the coil width, W, can be seen in Fig. 2. The flux lines are perpendicular to the flow direction on the active length, causing a field-dependent resistance.

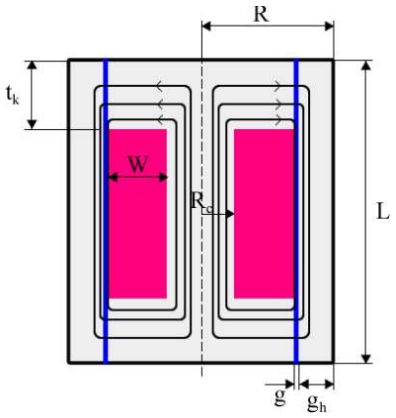

Fig. 2 Magnetic circuit of the MR damper

Since the magnetic field is applied, a few microns size particles dispersed in a carrying liquid form chains and the fluid becomes like a semi-solid material in a few milliseconds. This forming chain-like structure creates a resistance against the flow of the fluid, so that a rise in the fluid apparent viscosity occurs thanks to rising yield stress. MR fluid exhibits non-Newtonian behavior under the magnetic field.

Assuming that the pressure drop across the annular gap is equal to the pressure drop across the channel between the two parallel plates the pressure drop is calculated as follows.

$$\Delta P = \Delta P_\mu + \Delta P_\tau = \frac{6Q\mu L}{\pi R_1 g^3} + c\frac{2t_k}{g}\tau_y \qquad (1)$$

where ΔP_μ and ΔP_τ are the viscous (uncontrollable) and yield (controllable) pressure drop of MR damper. In the Eq.1, τ_y is yield stress, Q the flow rate, R_1 the average radius defining by $R_1 = R - (g_h + 0.5g)$ and c is the coefficient that depends on the flow velocity profile.

The total force generated by the damper, which consists of force due to the viscous effects F_μ, friction force F_f, and field-dependent force F_τ, is

$$F = F_\tau + F_\mu + F_f \qquad (2)$$

The dynamic range,D, is defined as the ratio of the total damping force to the uncontrollable force, which are the sum of the last two of Eq. 2.

$$D = 1 + \frac{F_\tau}{F_{\mu+}F_s} \qquad (3)$$

In the experimental design, four of the geometric dimensions of the MR damper shown in Fig. 2 were

determined as design parameters. The parameters were considered to have a significant effect on the damping force and the dynamic range in our previous works. damping force and dynamic range. 3 levels were determined for each parameter. These parameters and levels are shown in Table 1 below.

Table 1. The parameters and levels determined for MR damper

Parameters	Level 1	Level 2	Level 3
Gap (g)	0.4mm	0.6mm	0.8mm
Active length (t_k)	3mm	4mm	5mm
Radius of the piston core (R_c)	7mm	7.5mm	8mm
Gap length (L)	20mm	21mm	22mm

The levels of the parameter are distributed according to L9 orthogonal array of Taguchi experimental design method, can be seen in Table 2. The piston head radius and the piston head housing thickness were constant at 14.5 mm and 2 mm respectively. The values of coil width were determined with the equation $W = R - g - g_h - R_c$. In addition, since only geometric parameters would be examined in the study, 120 windings were made in the same coil thickness for all the dampers to neutralize the effect of all remaining parameters. Thus, 9 MR dampers were manufactured and tested (Fig. 3).

Table 2. The levels of the parameters assigned to L9 orthogonal array

	g	t_k	L	R_c
Damper 1	0.4	3	20	7
Damper 2	0.4	4	21	7.5
Damper 3	0.4	5	22	8
Damper 4	0.6	3	22	7.5
Damper 5	0.6	4	20	8
Damper 6	0.6	5	21	7
Damper 7	0.8	3	21	8
Damper 8	0.8	4	22	7
Damper 9	0.8	5	20	7.5

Fig. 3 One of manufactured dampers

To measure a quality characteristic and to determining optimum conditions was used type “bigger is better” of signal-to-noise ratio (S/N) to capture the variability of data in the group (Roy, 2003).

$$S/N = -10\log\left(\frac{1}{n}\sum\frac{1}{y_i^2}\right) \quad (4)$$

Assume that y_i is the i_{th} test value. If the S/N is increased it means of variation around the target value decreases, therefore, the desirability of S/N is always retained as bigger is better regardless of the original results. In the study each the damper was tested three times and the sum of the S/N calculations in Equation 4 was made for these three measurements.

III. TEST RESULTS

The manufactured dampers were tested on the machine of Roehrig MK-2150. The software of SHOCK 6.3 was used to to control the test machine and to collect data. A programmable “GWinstek PPE 3223” power supply was used to feed current to the MR damper. The temperature on the damper surface during the tests was measured by an IR temperature sensor on the machine. A load cell having a maximum capacity of 22 kN and a linear variable displacement transducer (LVDT) were used to measure the damping force and displacement of the piston rod of the MR damper, respectively. The relative velocity between the two ends of the shock absorber could also measured by LVDT. A heat sink as shown in Figure 4 was used to keep the damper temperature constant. Experimental set-up is shown in Fig. 4 with its main components.

Fig. 4 Test set-up for the dampers

The dynamic tests of the dampers was performed under the current varying at 1 A, while maintaining the piston maximum velocity and stoke at constant levels of 0.1 m/s and 20 mm, respectively. Force vs. time, force vs. displacement, and force vs. velocity curves were obtained in addition temperature, gas force, friction force for each test. All tests were performed at 30 °C of damper temperature. Temperatures of the MR dampers were measured by taking measurements made with a K-type thermocouple placed on the top of the active length on the inner side of the piston head. After each test, if the temperature was rising due to viscous, friction and current excitation, the damper was cooled by immersing in a temperature controlled box and 30 ($\mp$0.5)°C value was provided again. The maximum force values for each test were taken into account for the evaluations fallowing.

IV. MULTIPHYSICS NUMERICAL ANALYSIS OF FLUID FLOW AND MAGNETIC FIELD

The results at different velocities were obtained by numerical calculations in order to be able to evaluate the parameters of the MR damper at different velocities due to no available test data at different velocities.

Numerical analyzes of the MR dampers were carried out using the Magnetostatic and CFX tools of ANSYS 17.2. The coupled analyzes could be performed using a common grid for the whole flow area of the damper together with the solid volume of the piston affected by the magnetic field. Thus, both magnetic field analysis and computational fluid dynamics (CFD) solutions have been realized on the same solution grid. Values of the magnetic flux density obtained by magnetic field analysis were used to calculate apparent viscosity of MR fluid by Herchel-Bulkley model (Eq. 5) in CFD.

$$\mu = \frac{\tau_y}{\dot{\gamma}} + k\dot{\gamma}^{(n-1)} \qquad (5)$$

where μ is apperent viscosity of MR fluid, τ_y is yield stress depending on magnetic field, $\dot{\gamma}$ is shear rate, k and n are consistensy and flow index, respectively. A 20° part of the MR damper was analyzed to ensure the simulations faster and the lower cost. Steps for carrying out the coupled analysis are schematically shown in Figure 5.

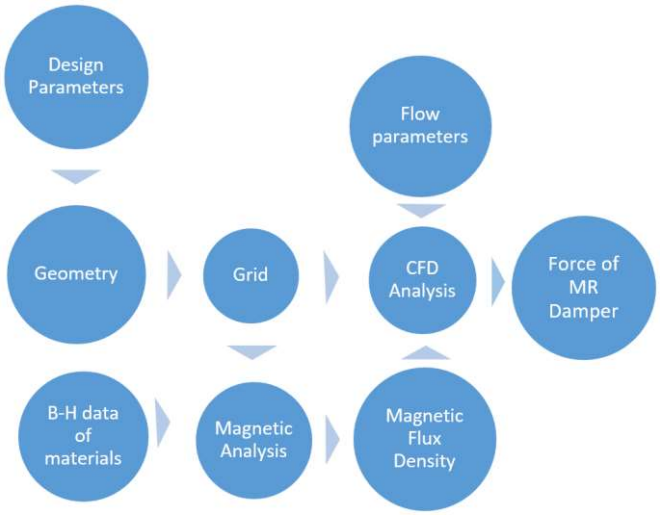

Fig. 5 Steps of the coupled analysis

The 3D CFD analyzes were carried out by CFX for an incompressible and non-Newtonian MR fluid,the momentum equation can be written as follows (ANSYS Documentation, 2016);

Navier–Stokes equations (momentum equations):

$$\frac{\partial(\rho U)}{\partial t} + \nabla(\rho U \times U) = -\nabla p + \nabla\tau \qquad (6)$$

where the stress tensor, τ, is related to the strain rate by

$$\tau = \mu\left(\nabla U + (\nabla U)^T - \frac{2}{3}\delta\nabla U\right) \qquad (7)$$

The magnetic flux density vs. magnetic field intensity (B-H) curves of the materials of the dampers, which are St37 steel and LORD MRF132-DG (Lord Technical Data, 2011), used in the tests were added in ANSYS 17.2 (Fig. 6).

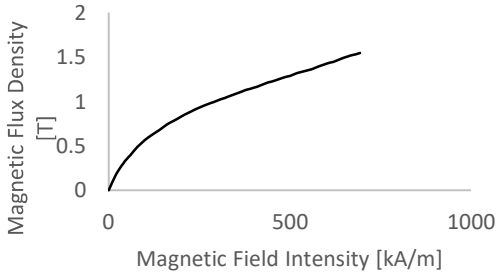

a.

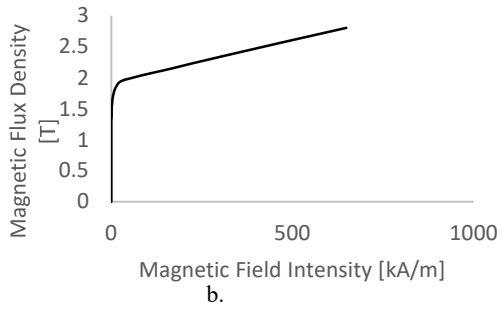

b.

Fig. 6 B-H curves of a. MRF132-DG b. St37 Steel

The solution grid with approximately 498000 elements depending on the design was used for each damper in the analyzed (Fig 7). The skewness of the mesh is 0.9, aspect ratio is 6.8775 and orthogonal quality is 0.994.

Fig. 7 The grid of coupled computational domain.

Compression and rebound movement of piston of the dampers could be modelled as in real work through the CFD analysis performed with deformed mesh and transient model. Therefore, flow magnitudes such as flow velocity, pressure, dynamic viscosity, force, shear rate, etc. could be obtained easily at any position of the piston. The deformed mesh, which can be defined as the self-realignment of the mesh according to the position of the last state by the time-dependent movement of surfaces defined as walls was provided that relationships of force-velocity and force-displacement could be compared with experimental results. While the piston was defined as stationary, the sinusoidal equation (Eq. 8) on appropriate to the experimental data was used for movement of the top and bottom surfaces of the cylinder. Movement of the bottom surface (the accumulator) was in accordance with the volume equal to the volume of covering or removing of piston rod.

$$x(t) = S_m(\cos(\omega t)) \qquad (8)$$
$$v(t) = V_m(\sin(\omega t))$$

where $x(t)$ and $v(t)$ are displacement and velocity, recpectively, $\omega = V_m/S_m$ is angular velocity, S is stroke. The analyzes were performed at 0.05m/s and 0.15m/s of maximum velocity (S_m) and at 0.02 m of maksimum stroke.

The values of the magnetic flux density from the magnetic field analysis at x, y and z coordinates of each node on the mesh were transferred to CFX as initials profile data, which can be seen in Figure 8.

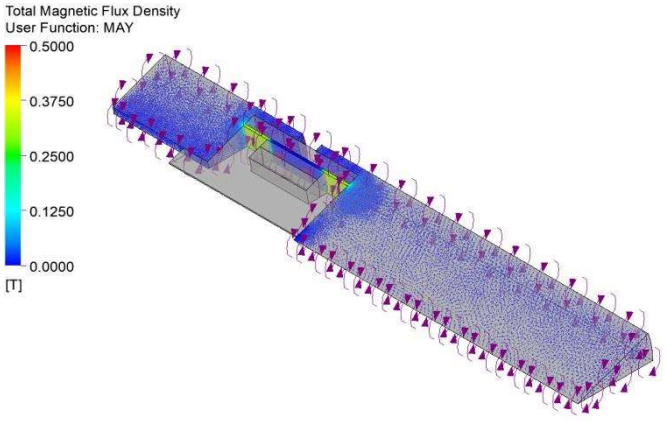

Fig. 8 Values of the magnetic flux density transferred from magnetic analysis on the flow domain

Behaviors of the MR fluid under applied current from 0 A to 5 A at from 20°C to 70°C were investigated by Anton Paar MCR 302 rheometer (Fig 9). The relationships of between yield stress and temperature are given in Fig 10. It is evident here that the yield stress, which significantly influences the viscosity of the fluid according to Eq. 5, varies considerably with temperature. In addition, this rate of change increases with increasing current. In this case, the CFD analyzes were carried out at a constant 30 °C temperature. The functions of the k, n and τ_y depending on magnetic flux density (Fig 11) were found by fitting relationship of Shear stress-Shear rate obtained the rheometer tests to the Herchel-Bulkley model given in Eq. 5 at constant 30°C. These values of k, n and τ_y for each node were also transferred to the CFX with the same initial profile data file.

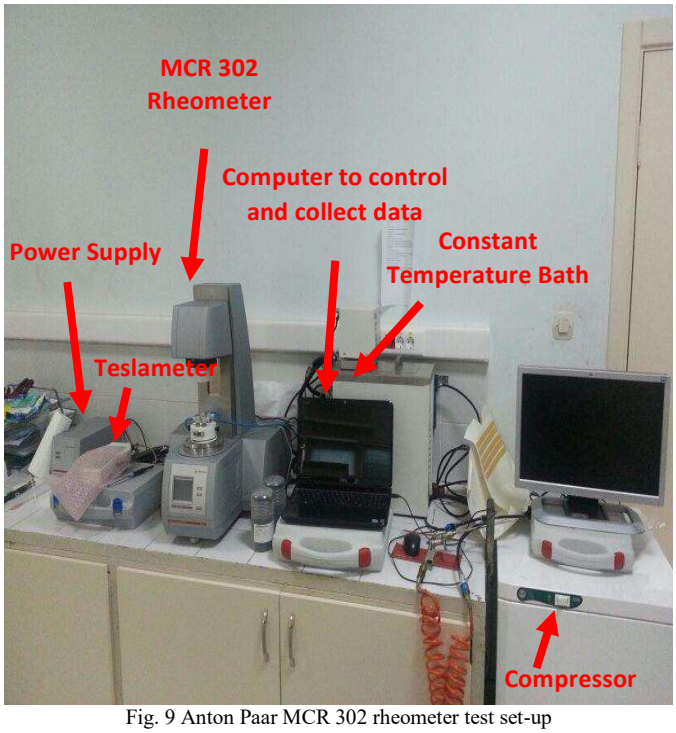

Fig. 9 Anton Paar MCR 302 rheometer test set-up

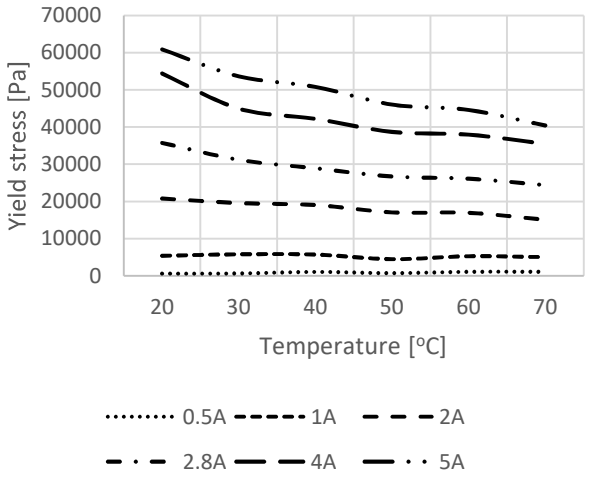

Fig. 10 The relationships of between yield stress (τ_y), and temperature

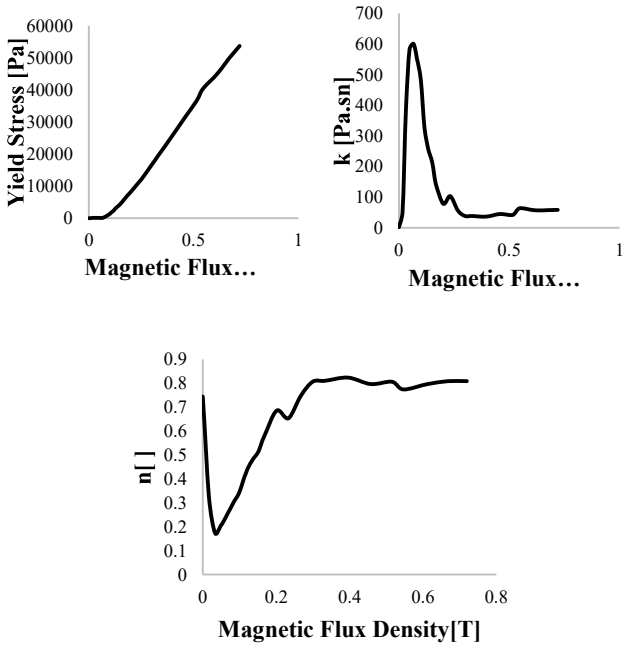

Fig. 11 The relationships of between magnetic flux density and τ_y,k and n for 30°C

The all the data was transferred to CFX as a variable called MAY, which could be used as an "Additional Variable" in CFX. Thus k, n, $\tau_y$and B were utilized to calculate viscosity of MR fluid by Eq. 5 for each node in flow domain. The viscosity varying with the applied magnetic field in the gap volume were handled especially to predict the damping force correctly. That some expressions such as various equations, numerical values and boundary conditions were defined in CFX made easy working on different velocity and stroke. The comparisons between The CFD analysis and the experimental results of the dampers for the maximum piston velocity of 0.1 m/s over the force –displacement graph are shown in Figure 12. In this way, CFD results were verified by experimental data when taking into consideration the maximum force values to be operated.

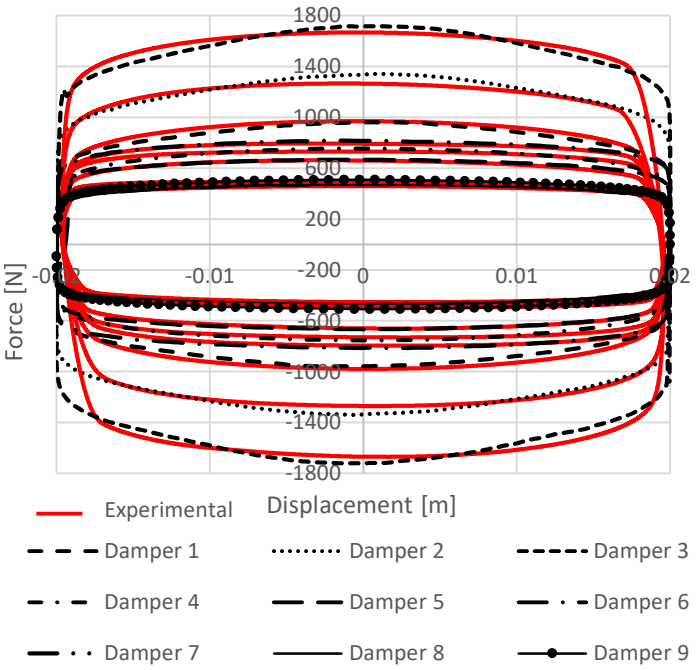

Fig. 12 The comparisons of CFD and Experimental results for 0.1 m/s

The new analyzes, which are at 1.0A and 0.02 m stroke, were conducted with the same validated CFD model for the velocities of 0.05 m/s and 0.15 m/s. The results of maximum force can be seen in Table 3.

Table 3. The coupled analysis results

	0.05 m/s		0.15 m/s	
	F [N]	D	F [N]	D
Damper 1	675.72	2.29	1272.10	2.41
Damper 2	978.30	2.64	1822.10	2.79
Damper 3	1265.64	3.06	2348.10	3.27
Damper 4	541.18	2.27	816.05	2.39
Damper 5	517.18	2.45	694.58	2.54
Damper 6	640.73	2.62	847.26	2.72
Damper 7	315.94	2.09	451.52	2.25
Damper 8	322.24	2.01	461.35	2.15
Damper 9	381.85	2.60	525.44	2.78

S/N ratios calculations (Table 4) made with these values in Table 8 and experimental results made for 0.1 m/s in above were realized to obtain the optimal levels of parameters and expected force and dynamic range.

Table 4. Optimal damper designs according to maximum force and dynamic range in terms of velocity

Velocity [m/s]	for	Optimal Levels				Expected Values		
		g	t	R_c	L	S/N	F [N]	D
0.05	F_{max}	1	3	3	3	62.05	1265.64	
	D_{max}	1	3	3	1	9.84		3.11
	F_{max} and D_{max}	1	3	2	2	37.54	785.36	4.07
0.1	F_{max}	1	3	3	3	64.53	1684.80	
	D_{max}	1	3	2	2	10.11		3.20
	F_{max} and D_{max}	1	3	2	3	37.55	785.51	4.07
0.15	F_{max}	1	3	2	3	67.59	2394.87	
	D_{max}	1	3	3	2	10.35		3.29
	F_{max} and D_{max}	1	3	2	3	37.90	798.37	4.14

According to these results, only level of the radius of piston core value at the velocity of 0.15 m/s was different compared to levels of the others in order to obtain the maximum damping force. The levels of the gap width and the active length remained the same as 1 and 3 respectively for each velocity and evaluation criterion. As a result, the optimal selections of levels of these two parameters is insensitive to velocity. According to the maximum force evaluation criteria, the gap length remained at level 3 which is largest value of the gap length. The expected force values could be obtained according to the maximum force criterion, but when two criterions are considered, this force showed a great decrease compared to the limited increase in the dynamic range. ANOVA results in terms of velocity can be seen in Table 5-7.

Table 5. ANOVA results for maximum force in terms of velocity

	P_g [%]	P_t[%]	P_{Rc}[%]	P_L[%]
0.05 m/s	86.44	9.19	1.79	2.57
0.1 m/s	89.13	4.78	1.71	4.38
0.15 m/s	92.00	4.06	1.43	2.51

As the speed increases, the effect of the gap width increased while the effect of the active length decreases in order to obtain the maximum force. Effect of the radius of piston core and the gap length remained almost constant.

Table 6. ANOVA results for maximum dynamic range in terms of velocity

	P_g [%]	P_t[%]	P_{Rc}[%]	P_L[%]
0.05 m/s	33.60	55.43	10.76	0.21
0.1 m/s	22.43	61.25	16.15	0.17
0.15 m/s	30.44	56.60	12.90	0.06

In order to obtain the maximum dynamic range, the most dominant parameter was the active length for all velocities, but the effects of all parameters remained almost constant with varying velocities.

Table 7. ANOVA results for maximum force and dynamic range in terms of velocity

	P_g [%]	P_t[%]	P_{Rc}[%]	P_L[%]
0.05 m/s	74.54	20.74	4.50	0.22
0.1 m/s	75.56	17.91	5.54	0.99
0.15 m/s	78.10	16.62	4.95	0.34

The gap width was the dominant parameter when looking at the maximum dynamic range and force, but the effects of all parameters remained almost constant with varying velocities.

V. CONCLUSION

In this study, an experimental design was performed for the MR damper with specified parameters, which are the gap width, the active length, the gap length and the radius of piston core. The tests of manufactured the nine dampers were made under constant damping velocity at constant 30°C with checking by the thermocouples placed in the piston head because varying temperatures affect the performance of the damper significantly and the damper reacts different responses. The optimal levels of the design parameters were obtained for the objective of the maximum damping force and/or maximum dynamic range. Also, effects of each parameter on the maximum damping force and/or maximum dynamic range were calculated by the variance analysis. The coupled numerical model confirmed by experimental data was developed and the magnetic field and time-dependent CFD analyzes were performed on the same geometry to obtain the damping force values under different velocities. The analysis showed that;

- The effect of the gap width, which is most dominant, increased with the increasing velocity by just 5.56 %, while the effect of the active length decreases by 5.13% to achieve the maximum damping force.
- The effects of all of the parameters were almost unchanged with velocity for maximum dynamic range. The result pointed that the effect of the all parameters did not also change with the velocity to achieving maximum force and dynamic range together.

REFERENCES

ANSYS Documentation (2016) ANSYS CFX Theory Guide. *ANSYS Help.*

Azraai MR, Priyandoko G, Yusoff A R and Rashid MFFA (2015) Parametric Optimization of magneto-rheological fluid damper using particle swarm optimization. *International Journal of Automotive and Mechanical Engineering* 11:2591.

Erol O and Gurocak H (2011) Interactive design optimization of magnetorheological-brake actuators using the taguchi method. *Smart Materials and Structures*, 20(10): 105027 (12pp).

Hitchcock GH (2002) *A Novel Magneto-rheological Fluid Damper*. Master thesis, Mechanical Engineering Department, University of Nevada, Reno.

Hu G, Liu F, Xie Z and Xu M (2016) Design, analysis, and experimental evaluation of a double coil magnetorheological fluid damper. *Shock and Vibration* 4184726 (12 pp).

Karakoc K, Park EJ and Suleyman A (2008) Design considerations for an automotive magnetorheological brake. *Mechatronics* 18(8): 434-447.

Kemerli, M, Engin, T and Parlak Z (2019) Coupled Magnetic and CFD Modelling of a Structural Magnetorheological Vibration Absorber with Experimental Validation. *In Mechanism, Machine, Robotics and Mechatronics Sciences* (pp. 115-125). Springer, Cham.

Lord Technical Data (2011) MRF-132DG Magneto-Rheological Fluid. Available at: http://www.lordmrstore.com/_literature_231215/Data_Sheet_-_MRF-132DG_Magneto-Rheological_Fluid, (accessed 2 June 2018).

Nguyen QH, Han YM, Cho SB and Wereley NM (2007) Geometry optimization of MR valves constrained in a specific volume using the finite element method. *Smart Materials and Structures* 16 (6): 2242-2252.

Parlak Z, Engin T and Şahin İ (2013) Optimal magnetorheological damper configuration using the Taguchi experimental design method. *Journal of Mechanical Design* 135(8): 081008 (9pp).

Parlak Z, Engin T. (2012) Time-dependent CFD and quasi-static analysis of magnetorheological fluid dampers with experimental validation. *International Journal of Mechanical Sciences* 64(1): 22-31.

Rosenfeld NC and Wereley NM (2004) Volume-constrained optimization of magnetorheological and electrorheological valves and dampers. *Smart Materials and Structures* 13(6): 1303-1313.

Roy RK (2003) Design Experiments Using the Taguchi Aproach:16 Steps to Product and Process. Improvement. New York: A Wiley–Interscience Publication.

Sternberg A, Zemp R, de la Llera JC. (2014) Multiphysics behavior of a magneto-rheological damper and experimental validation. *Engineering Structures* 69:194-205.

Thirupathi P, Janaki RP, Venukumar S, Saikiran RP, Krishna RB, and Battacharya S (2015) Experimental Analysis of MR Fluid by Magneto-Rheological (MR) Damper. *Applied Mechanics and Materials* 813-814: 1002-1006

Yu G, Du C and Sun T (2015) Thermodynamic behaviors of a kind of self-decoupling magnetorheological damper. *Shock and Vibration* 502747 (9 pp).

Zheng J, Li Y, Li Z and Wang J (2015) Transient multi-physics analysis of a magnetorheological shock absorber with the inverse Jiles–Atherton hysteresis model. *Smart Materials and Structures* 24(10): 105024 (16pp)

Zhu X, Wang W, Yao B, Cao J and Wang Q (2015) Analytical modeling and optimal design of a MR damper with power generation. In: *AIM 2015 - IEEE International Conference on Advanced Intelligent Mechatronic*, Busan, Korea, 7-11 July 2015, pp. 1531-1536. IEEE